Monthly Notices
of the
ROYAL ASTRONOMICAL SOCIETY

MNRAS **492,** 45–57 (2020)
Advance Access publication 2019 December 10

doi:10.1093/mnras/stz3445

Sardinia Radio Telescope observations of Local Group dwarf galaxies – I. The cases of NGC 6822, IC 1613, and WLM

A. Tarchi,[1★] P. Castangia,[1★] G. Surcis,[1] A. Brunthaler,[2] C. Henkel,[2,3] M. Pawlowski,[4] K. M. Menten,[2] A. Melis,[1] S. Casu,[1] M. Murgia,[1] A. Trois,[1] R. Concu[1] and J. Darling[5]

[1]*INAF – Osservatorio Astronomico di Cagliari, Via della Scienza 5, I-09047 Selargius (CA), Italy*
[2]*Max-Planck-Institut für Radioastronomie, Auf dem Hügel 71, D-53121 Bonn, Germany*
[3]*Astronomy Departement, King Abdulaziz University, PO Box 80203, Jeddah 21589, Saudi Arabia*
[4]*Leibniz-Institut für Astrophysik Potsdam, An der Sternwarte 16, D-14482 Potsdam, Germany*
[5]*Center for Astrophysics and Space Astronomy, Department of Astrophysical and Planetary Sciences, University of Colorado, 389 UCB, Boulder, CO 80309-0389, USA*

Accepted 2019 December 4. Received 2019 December 4; in original form 2019 November 6

ABSTRACT

Almost all dwarf galaxies in the Local Group (LG) that are not satellites of the Milky Way or M 31 belong to either one of two highly symmetric planes. It is still a matter of debate whether these planar structures are dynamically stable or whether they only represent a transient alignment. Proper motions, if they could be measured, could help to discriminate between these scenarios. Such motions could be determined with multi-epoch very long baseline interferometry (VLBI) of sources that show emission from water and methanol at frequencies of 22 and 6.7 GHz, respectively. We report searches for such masers. We have mapped three LG galaxies, NGC 6822, IC 1613, and WLM, in the bands covering the water vapour and methanol lines. These systems are members of the two above-mentioned planes of galaxies. We have produced deep radio continuum (RC) maps and spectral line cubes. The former have been used to identify star-forming regions and to derive global galactic star formation rates (SFRs). These SFRs turn out to be lower than those determined at other wavelengths in two of our sources. This indicates that dwarf galaxies may follow predictions on the RC–SFR relation only in individual regions of enhanced RC emission, but not when considering the entire optical body of the sources. No methanol or water maser emission has been confidently detected, down to line luminosity limits of $\sim 4 \times 10^{-3}$ and 10×10^{-3} $L_{\odot}$, respectively. This finding is consistent with the small sizes, low SFRs, and metallicities of these galaxies.

Key words: masers – galaxies: dwarf – Local Group – radio continuum: galaxies – radio lines: ISM.

1 INTRODUCTION

The dwarf galaxies in the Local Group (LG), the only galaxy ensemble for which accurate 3D positions are known, reveal a surprising amount of spatial structure. The satellite galaxies of the Milky Way (MW) lie within a vast polar structure (VPOS), a thin (28 kpc root-mean-square – rms – height) plane extending to a Galactocentric distance of 250 kpc (Pawlowski, Pflamm-Altenburg & Kroupa 2012). Similar planes of satellites surround M31 (Ibata et al. 2013) and Centaurus A (Müller et al. 2018). In addition to these satellite galaxy planes, the distribution of dwarf galaxies in the LG reveals further structuring (Pawlowski, Kroupa & Jerjen 2013). Almost all other LG dwarfs belong to either one of two planes, termed LG plane 1 (10 galaxies) and LG plane 2 (7 galaxies). The most puzzling feature of the last two planes is their pronounced symmetry. Both planes have large diameters (1.5–2 Mpc), but are extremely thin (32.5 ± 1.9 and 59.9 ± 4.0 kpc, respectively). They both are inclined by only ≈19° with respect to the stellar disc of M31, but by 30° relative to each other. In addition, both planes (1 and 2) have essentially the same offset (≈190 kpc) from the MW and from M31; i.e. they are both almost parallel to the line connecting the MW and M31. If all these structures in the LG were dynamically stable, then the galaxies would move within the associated plane, which would allow us to predict the expected proper motion of individual satellites in such structures (Pawlowski & Kroupa 2013; Pawlowski, McGaugh & Jerjen 2015). Otherwise, the structures may only represent transient alignments that would disperse as the dwarf galaxies continue their independent motions, as expected from cosmological simulations (e.g. Gillet

★ E-mail: andrea.tarchi@inaf.it (AT); paola.castangia@inaf.it (PC)

et al. 2015; Buck et al. 2016). For the VPOS of the MW, this can be tested using optical proper motion measurements, revealing that indeed most of the classical MW satellites co-orbit in the (VPOS) plane (Metz, Kroupa & Libeskind 2008; Pawlowski & Kroupa 2013; Fritz, Battaglia & Pawlowski 2018; Gaia Collaboration 2018). Likewise, the favourable edge-on orientation of the M31 satellites as seen from the MW allowed (Ibata et al. 2013) to use only radial velocities (hereafter, to be understood as line-of-sight velocities) to demonstrate that 13 of the 15 satellites in the plane are consistent with co-orbiting motion. Unfortunately, information on the motions of dwarf galaxies belonging to the two LG planes (1 and 2) is not easily available. These planes are not seen edge-on, rendering radial velocities alone inconclusive, and optical proper motion measurements are currently not feasible due to the large distances of these objects.

For nearby galaxies, a viable method to derive proper motions is offered by very long baseline interferometry (VLBI) studies of the 22-GHz water maser line in star-forming regions. Indeed, VLBI observations of water maser spots in phase-referencing mode allow us to measure the 3D motions of the host galaxies with respect to distant quasars. In addition, distance measurements are possible by applying the rotational parallax method to the detected maser spots with relevant implications for cosmological parameters and the total mass of matter (luminous and dark) of the LG. So far, such studies have been successfully performed on a limited number of maser spots detected in the galaxies M 33 and IC 10 (e.g. Greenhill et al. 1993; Brunthaler et al. 2005; Brunthaler et al. 2007). In particular, the measurement performed on IC 10 shows the potential lying in such studies for our case. This galaxy belongs to the LG plane 2, with a distance from the best-fitting plane of only 37 ± 13 kpc (0.62 ± 0.22 rms heights). In addition to its radial velocity, IC 10's proper motion has been measured using water masers (Brunthaler et al. 2007). The resulting velocity vector of the galaxy aligns to better than 10° with the LG plane 2, demonstrating the possible dynamical association of this dwarf galaxy with its plane. Alternatively, also methanol maser lines can be used for proper motion studies. This possibility, for extragalactic studies, has been further supported by the detection of methanol maser sources in M31 (Sjouwerman et al. 2010).

Within the aforementioned framework, it is particularly important to detect as many water/methanol maser sources as possible in any galaxy belonging to the LG and, in particular, in the LG dwarf galaxies belonging to the LG planar structures 1 and 2. Until recently, water maser sources in the LG were found only in M 33 (3 sources), IC 10 (2 sources), the LMC (30 sources), and the SMC (6 sources; see Henkel et al. 2018, and references therein). Possible causes for this low detection rate can be both the difficulty to map the entire body of the galaxies and the limited sensitivity of the observational campaigns. The former motivation is especially dramatic for M 31 that covers (due to its size and proximity) a huge area of the sky (120 arcmin $\times$ 40 arcmin). Indeed, at the end of 2010, the first detection of maser emission in five (out of 206) 24 μm selected regions in M31 has been obtained with the Green Bank Telescope (GBT; Darling 2011). A few months earlier, the detection of methanol maser emission was reported by Sjouwerman et al. (2010) in the disc of M31. However, the lack of a counterpart at another wavelength was sometimes reported in maser detections (see e.g. Becker et al. 1993 for IC 10-NW; Amiri & Darling 2016 for one case in M 31). This strongly motivates un-biased searches for maser sources in fully sampled spectroscopic images rather than focusing only on well-known isolated hotspots.

This paper reports the first results of a large project, carried out with the Sardinia Radio Telescope (SRT), aimed at mapping the radio continuum (RC) and spectral line emission at *C* ($\lambda \sim 5$ cm) and *K* ($\lambda \sim 1.3$ cm) bands from 14 (out of a total of 17) LG dwarf galaxies belonging to the LG planar structures 1 and 2, and being visible at the SRT latitude (and excluding IC 10). The final aim of the project is that of obtaining spectro-polarimetric maps of the full optical body[1] of the galaxies with the SRT at a resolution of about 3 and 1 arcmin, at *C* and *K* bands, respectively. The main scientific goals are (i) to detect spectral line emission in the observed band, in particular from the 6.7-GHz methanol and 22-GHz water maser lines and to locate them with high enough precision for interferometric follow-up studies and (ii) to obtain deep and full polarization maps of the RC emission. These will provide relevant clues on individual star-forming regions hosting groups of thermal (compact or regular H II regions) and non-thermal (radio supernovae and supernova remnants) sources present in the target galaxies. This work reports the details of the observations and data reduction (Section 2), and summarizes the main results achieved on the first three galaxies analysed, so far, NGC 6822, IC 1613, and WLM (Section 3). Section 4 provides a discussion on the interpretation of the intensity and distribution of the RC sources, and of the number of maser detections found in the three targets. The last section itemizes the main conclusions produced by the first part of this large project. The results for the other galaxies in the sample, together with a more comprehensive study of the sample, will be the subject of a subsequent paper (Paper II).

2 OBSERVATIONS AND DATA REDUCTION

Observations were performed with the SRT (Bolli et al. 2015; Prandoni et al. 2017, and references therein) in the framework of the Early Science Program (ESP) that started on 2016 February 1 and lasted for about six months.

Our project, labelled ESP-S0003 (220 h; PI: A. Tarchi), aimed at mapping the full extension of 14 (out of a total of 17) LG dwarf galaxies belonging to the LG planar structures 1 and 2 that were visible at the SRT latitude (excluding IC 10). We used the *C* and *K* bands receivers[2] in conjunction with the SARDARA, ROACH2-based digital backend (Melis et al. 2018). At *C* band, we observed with an actual bandwidth (BW) of 1.2 GHz centred around 6.6 GHz, in order to cover both methanol and excited OH maser line transitions (near 6.7 and 6.0 GHz, respectively), while trying to avoid strong RFI present at 5.9 GHz. At *K* band, the 1.2-GHz actual band was centred close to (but not coincident with)[3] the frequency of the main water maser line (rest frequency 22.235 08 GHz) Doppler-shifted by the systemic heliocentric velocity of the targets (taken by McConnachie 2012). We used the 1.5-GHz (nominal) band SARDARA configuration with 16 384 channels, yielding a

[1]Defined by the major angular diameter in arcminutes, corresponding to the Holmberg isophote ($26^{m}.5\,\mathrm{arcsec}^{-2}$) in the *B* band (Karachentsev, Makarov & Kaisina 2013).

[2]At *K* band, only the central feed of the 7-feed receiver was used in our observations, since, at that time, only this feed was offered in conjunction with the SARDARA backend.

[3]We centred the band with an offset of 15 MHz towards lower frequencies, w.r.t. the frequency of the main water maser line Doppler-shifted by the systemic heliocentric velocity of the targets. This was done in order to avoid to centre the possible systemic line on a strong birdie, known to be present in the central channel.

Table 1. Target name and coordinates, LG plane to which the galaxy seems to belong (see Section 1), distance, and optical size.

Source	RA (J2000)	Dec. (J2000)	LG plane	D^a (kpc)	Optical size^b (arcmin)
NGC 6822	$19^h44^m57.7^s$	$-14^d48^m12^s$	2	490 ± 40	19.05
IC 1613	$01^h04^m47.8^s$	$+02^d07^m04^s$	1	700 ± 35	19.05
WLM	$00^h01^m58.1^s$	$-15^d27^m39^s$	1	925 ± 40	11.48

[a]From Mateo (1998).
[b]Major angular diameter in arcminutes, corresponding the Holmberg isophote in the *B* band (from Karachentsev et al. 2013).

frequency resolution of ∼91 kHz (≈4 and 1.2 km s^{-1}, at and *K* bands, respectively).

The spectroscopic check of the system was done by observing, in position-switching mode, the strong methanol and water maser emission in the well-known source W3(OH). All maps were performed using the on-the-fly (OTF) mapping technique using scan speeds between 3° min^{-1} (at *C* band) and 1–3° min^{-1} (at *K* band, depending on the size of the map; the smaller the map, the lower the speed). At *C* band, we mapped, for all galaxies, square regions of 21 arcmin × 21 arcmin centred on the target coordinates (J2000 epoch), as reported in the NASA/IPAC Extragalactic Database (NED). The area was covered with 29 scans (in each direction) separated by 45 arcsec along both RA and Dec., with an acquisition rate of ∼30 spectra s^{-1}, thus properly sampling the ∼3 arcmin SRT beam at *C* band. At *K* band, the size of the regions observed depends on the optical size of the galaxy. For NGC 6822 and IC 1613, we mapped a region of 18 arcmin × 18 arcmin with a 15 arcsec separation along both RA and Dec. (thus 73 scans, in each direction), while for WLM a 12 arcmin × 12 arcmin sized map with a 15 arcsec separation (49 scans, in each direction) was performed. The size of the maps at *C* band included the full optical body of all three galaxies (see Table 1). At *K* band, the whole optical extent of the galaxy WLM was mapped, while for the most extended targets, NGC 6822 and IC 1613, the maps were slightly smaller with respect to (w.r.t.) the optical major axis, namely 18 arcmin versus 19 arcmin (see Table 1). The acquisition rate was ∼60 spectra s^{-1} sufficient to have a proper sampling of the ∼1 arcmin SRT beam at *K* band. Multiple maps along RA and Dec. were performed for each galaxy that were later averaged to increase the final sensitivity. Table 2 reports all the details of the observations.

The data were calibrated by using the proprietary Single-dish Spectral-polarimetry Software (SCUBE; Murgia et al. 2016). The name of the observed calibrators are reported in Table 2, together with an indication on which of them were used for the flux and/or polarization calibration. The steps of the data reduction, including flux density, polarization calibration, and RFI flagging for a standard spectro-polarimetric OTF SRT data set are thoroughly described in Murgia et al. (2016; their Section 3) and Govoni et al. (2017; their section 3.1). Hence, with the exception of possible peculiar problems related to the data reduction of our project, the steps will not be repeated here. In addition, with SCUBE we have also performed total intensity and polarization imaging using the methods described in Murgia et al. (2016, their sections 4.1 and 4.3) and Govoni et al. (2017, their sections 3.1.1 and 3.1.2). Unfortunately, the polarization calibration at *K* band failed, due to problems under investigation, and hence, only polarization imaging at *C* band is reported and discussed in this paper.

We created total intensity image cubes of all 16 384 channels both at *C* and *K* bands, and produced RC images by averaging the inner 80 per cent of the whole bands, after removing the channels where birdies are known to be present. Cubes at different epochs were re-aligned in velocity using SCUBE, in order to account for the Doppler shift introduced by the Earth rotation. The proper velocities were computed by using 'offline' the FTRACK software (Orlati et al., in preparation) developed for the Italian radio telescopes and not yet implemented for SARDARA backend acquisitions at the time of the observations. For each source, cubes at different epochs were finally averaged and the averaged cubes searched for methanol and water maser line features using the following method and criteria:

(i) we used the first step of the identification process described in Surcis et al. (2011, their section 3.1). This implies the use of a program called 'maser finder' (developed by S. Curiel), which is able to search for maser spots, velocity channel by velocity channel, with a signal-to-noise ratio (SNR) greater than a given value (in our case, a 5σ limit was used);
(ii) we limited our search to a frequency window corresponding to a range in velocity of ±200 km s^{-1}, centred on the frequency at which the 6.7-GHz methanol and 22-GHz water maser line is expected due to the systemic heliocentric velocity of the galaxy (taken from McConnachie 2012);
(iii) we collected all candidate maser features found in the process;
(iv) we considered as detections those candidate maser features whose peak flux density exceeds by seven times the rms found in the spectrum at the position of the feature;
(v) we considered as tentative detections those candidate maser features whose peak flux density was between four and seven times the rms found in the spectrum at the position of the feature (see also Appendix A).

The analysis of the RC and spectral line maps was mainly led utilizing standard tasks implemented in the NRAO Astronomical Image Processing System (AIPS[4]).

The overlays presented in Section 4.1 were produced using the 'kvis' image/movie viewer in the KARMA software.[5]

3 RESULTS

Figs 1–3 show the total intensity RC maps of the three target galaxies, NGC 6822, IC 1613, and WLM obtained from our SRT observations at *C* and *K* bands. There is evidence of a number of emitting spots above an average 3σ level in our maps of about 2 and 6 mJy beam^{-1} for the *C* and *K* bands, respectively. Peak and integrated flux densities are reported in Tables 3–5. The estimated systemic uncertainty on the absolute flux density calibration for

[4]http://www.aips.nrao.edu
[5]https://www.atnf.csiro.au/computing/software/karma/index.html

Table 2. Details of the SRT observations.

Source	Frequency (MHz)	Obs. date (yyyy-mm-dd)	OTF maps (nRA × nDec.)	Mapping time[a] (h)	Observed calibrators[b]
NGC 6822	6001–7201	2016-04-01	19 × 19	5.0	3C 48, *3C 286*, 3C 295, NGC 7027
NGC 6822	21 574–22 774	2016-03-30	8 × 8	5.1	3C 48, *3C 286*, 3C 295, NGC 7027
NGC 6822	21 574–22 774	2016-04-03	7 × 7	4.5	3C 48, *3C 286*, NGC 7027
NGC 6822	21 574–22 774	2016-04-10	5 × 5	3.2	3C 48, 3C 147, *3C 286*, NGC 7027
NGC 6822	21 574–22 774	2016-04-13	9 × 9	5.8	3C 48, *3C 286*, 3C 295, NGC 7027
NGC 6822	21 574–22 774	2016-04-15	8 × 8	5.1	3C 48, *3C 286*, 3C 295, NGC 7027
NGC 6822	21 574–22 774	2016-04-16	9 × 9	5.9	3C 48, *3C 286*, 3C 295, NGC 7027
NGC 6822	21 574–22 774	2016-04-17	9 × 9	5.8	3C 48, *3C 286*, 3C 295, NGC 7027
NGC 6822	21 574–22 774	2016-04-19	5 × 5	3.2	*3C 286*, NGC 7027
IC 1613	6005–7202	2016-03-12	16 × 16	4.2	3C 138, *3C 147*, NGC 7027
IC 1613	6005–7202	2016-04-01	8 × 8	5.1	*3C 48*, 3C 138, NGC 7027
IC 1613	6042–7202	2016-04-02	5 × 5	3.2	*3C 48*, 3C 138, NGC 7027
IC 1613	21 588–22 788	2016-04-13	6 × 6	3.8	*3C 48*, NGC 7027
IC 1613	21 588–22 788	2016-04-15	5 × 5	3.2	*3C 48*, 3C 138, NGC 7027
IC 1613	21 588–22 788	2016-04-16	6 × 6	3.8	*3C 48*, NGC 7027
IC 1613	21 588–22 788	2016-04-17	6 × 6	3.8	*3C 48*, NGC 7027
IC 1613	21 588–22 788	2016-04-19	6 × 6	3.8	*3C 48*, 3C 147, NGC 7027
IC 1613	21 588–22 788	2016-04-20	5 × 5	3.2	*3C 48*, 3C 147
IC 1613	21 588–22 788	2016-04-22	8 × 8	5.1	*3C 48*
WLM	6002–7202	2016-03-13	5 × 5	1.3	*3C 48*, 3C 138, NGC 7027
WLM	6002–7202	2016-04-10	12 × 12	3.2	3C 84, 3C 138, *3C 147*
WLM	21 569–22 769	2016-04-27	14 × 14	6.0	3C 138, *3C 147*, 3C 295
WLM	21 569–22 769	2016-05-24	9 × 9	3.8	3C 138, *3C 147*, NGC 7027
WLM	21 569–22 769	2016-05-25	11 × 11	4.7	3C 138, *3C 147*, NGC 7027

[a]Including overheads (acceleration and deceleration during scans).
[b]Sources used for flux calibration are marked in italics. Polarization angle was calibrated using 3C 286 (for NGC 6822) and 3C 138 (for IC 1613 and WLM). For all three targets, polarization leakage was calibrated using NGC 7027, with the exception of one *K*-band epoch of WLM, for which 3C 84 was employed.

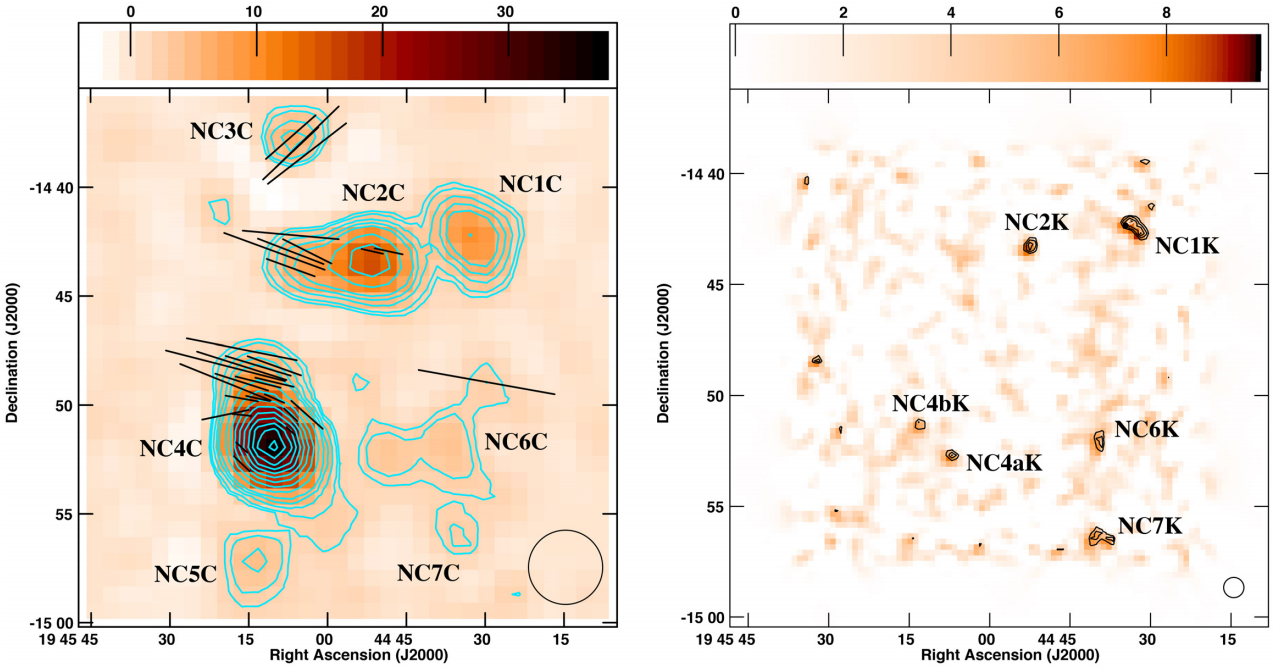

Figure 1. *Left:* SRT *C*-band total intensity 21 arcmin × 21 arcmin image of NGC 6822 resulting from the spectral average of the inner 80 per cent of the bandwidth. The FWHM beam is 2.9 arcmin (bottom-right corner). The noise level is 0.65 mJy beam^{-1}. Contour levels are 0.65 × (3, 4, 6, 8, 10, 15, 20, ..., 80) mJy. Electric field polarization vectors are overlaid. The length of the vectors is proportional to the polarization percentage (with 10 per cent being a bar of ∼2.1 arcmin), while their orientation represents the polarization angle. The error on the polarization angle is less than 10°, and the fractional polarization is above $3\sigma_{\rm FPOL}$. *Right:* SRT *K*-band total intensity 18 arcmin × 18 arcmin image of NGC 6822 resulting from the spectral average of the inner 80 per cent of the bandwidth. The FWHM beam is 0.9 arcmin (bottom-right corner). The noise level is 2.0 mJy beam^{-1}. Contour levels are 2.0 × (3, 3.5, 4, 4.5, 5, 6, 7) mJy.

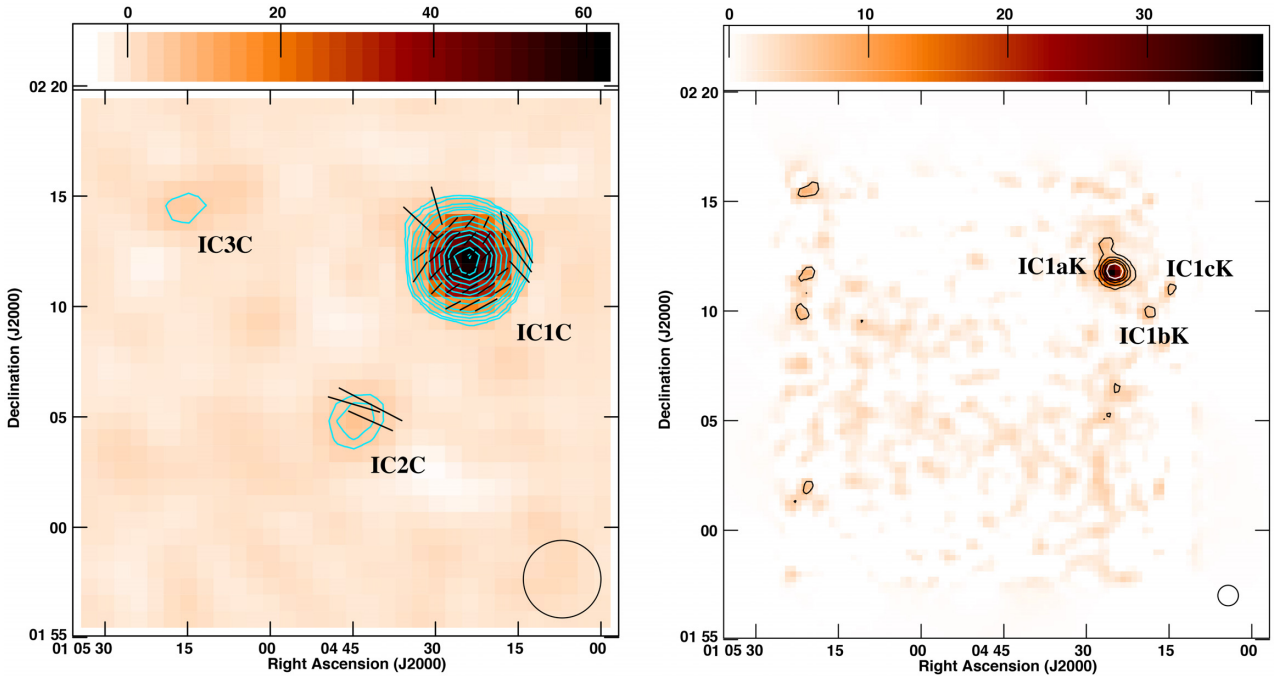

Figure 2. *Left:* SRT *C*-band total intensity 21 arcmin × 21 arcmin image of IC 1613 resulting from the spectral average of the inner 80 per cent of the bandwidth. The FWHM beam is 2.9 arcmin (bottom-right corner). The noise level is 1.0 mJy beam^{-1}. Contour levels are 1.0 × (3, 4, 6, 8, 10, 15, 20, ..., 80) mJy. Electric field polarization vectors are overlaid. The length of the vectors is proportional to the polarization percentage (with 10 per cent being a bar of ∼2.1 arcmin), while their orientation represents the polarization angle. The error on the polarization angle is less than 10°, and the fractional polarization is above $3\sigma_{\rm FPOL}$. *Right:* SRT *K*-band total intensity 18 arcmin × 18 arcmin image of IC 1613 resulting from the spectral average of the inner 80 per cent of the bandwidth. The FWHM beam is 0.9 arcmin (bottom-right corner). The noise level is 1.7 mJy beam^{-1}. Contour levels are 1.7 × (3, 6, 9, 12, 15) mJy.

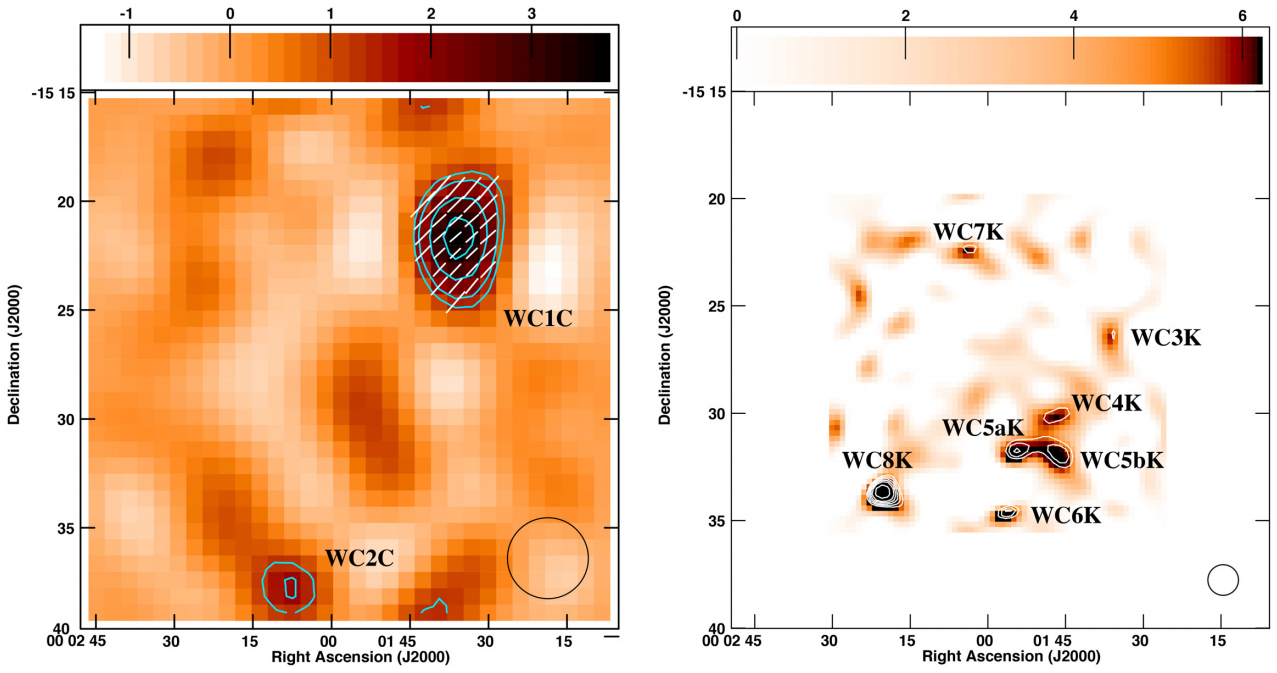

Figure 3. *Left:* SRT *C*-band total intensity 21 arcmin × 21 arcmin image of WLM resulting from the spectral average of the inner 80 per cent of the bandwidth. For this source, the original beam was convolved to an FWHM size of 3.75 arcmin (bottom-right corner). The noise level is 0.4 mJy beam^{-1}. Contour levels are 0.4 × (3, 4, 6, 8, 10, 10, 15, 20, ..., 80) mJy. Electric field polarization vectors are overlaid. The length of the vectors is proportional to the polarization percentage (with 50 per cent being a bar of ∼0.75 arcmin), while their orientation represents the polarization angle. The error on the polarization angle is less than 10°, and the fractional polarization is above $3\sigma_{\rm FPOL}$. *Right:* SRT *K*-band total intensity 12 arcmin × 12 arcmin image of WLM resulting from the spectral average of the inner 80 per cent of the bandwidth. For this source, the original beam was convolved to an FWHM size of 1.4 arcmin (bottom-right corner). The noise level is 1.9 mJy beam^{-1}. Contour levels are 1.9 × (3, 3.5, 4, 4.5, 5, 6, 7) mJy.

Table 3. Continuum sources detected in NGC 6822: label, coordinates, peak and integrated flux density, and spectral index between 1.4 and 22 GHz (with $S \propto \nu^{\alpha}$) derived for those sources detected with the SRT at *K* band having a counterpart in the NVSS (see Section 4.1).

Label	RA (J2000)	Dec. (J2000)	Peak (mJy beam^{-1})	Integrated (mJy)	$\alpha_{1.4}^{22}$
NC1C	19 44 32.8 ± 0.4	− 14 42 21 ± 6	10.8 ± 0.6	10.8 ± 0.6	
NC2C	19 44 52.3 ± 0.2	− 14 43 27 ± 3	17.4 ± 0.9	21 ± 1	
NC3C	19 45 06.5 ± 0.9	− 14 37 31 ± 13	4.7 ± 0.6	4.7 ± 0.6	
NC4C	19 45 10.7 ± 0.1	− 14 51 45 ± 1	41 ± 2	48 ± 2	
NC5C	19 45 13.5 ± 0.9	− 14 57 20 ± 13	4.6 ± 0.6	4.6 ± 0.6	
NC6C	19 44 36.9 ± 0.9	− 14 52 04 ± 13	4.6 ± 0.6	8 ± 1	
NC7C	19 44 35.0 ± 1.4	− 14 55 24 ± 20	3.0 ± 0.6	3.0 ± 0.6	
NC1K	19 44 33.378 ± 0.005	− 14 42 18.35 ± 0.07	11 ± 2	11 ± 3	0.1 ± 0.1
NC2K	19 44 52.459 ± 0.006	− 14 43 14.99 ± 0.09	8 ± 2	8 ± 2	− 0.3 ± 0.1
NC4aK	19 45 07.267 ± 0.007	− 14 52 42.0 ± 0.1	7 ± 2	7 ± 2	− 0.6 ± 0.1
NC4bK	19 45 13.212 ± 0.007	− 14 51 26.17 ± 0.09	8 ± 2	8 ± 2	− 1.1 ± 0.1
NC6K	19 44 39.666 ± 0.006	− 14 51 53.89 ± 0.08	9 ± 2	9 ± 2	–
NC7K	19 44 39.661 ± 0.005	− 14 56 27.24 ± 0.07	10 ± 2	10 ± 3	–

Table 4. Continuum sources detected in IC 1613: label, coordinates, peak and integrated flux density, and spectral index between 1.4 and 22 GHz (with $S \propto \nu^{\alpha}$) derived for those sources detected with the SRT at *K* band having a counterpart in the NVSS (see Section 4.1).

Label	RA (J2000)	Dec. (J2000)	Peak (mJy beam^{-1})	Integrated (mJy)	$\alpha_{1.4}^{22}$
IC1C	01 04 24.20 ± 0.07	02 12 05 ± 1	65 ± 3	65 ± 3	
IC2C	01 04 44.7 ± 0.8	02 04 49 ± 12	6 ± 1	6 ± 1	
IC3C	01 05 12.6 ± 1.1	02 14 40 ± 17	4 ± 1	4 ± 1	
IC1aK	01 04 24.836 ± 0.005	02 11 48.83 ± 0.08	41 ± 6	49 ± 7	−0.12 ± 0.05
IC1bK	01 04 18.35 ± 0.04	02 10 03.0 ± 0.5	6.3 ± 1.7	6.3 ± 1.7	–
IC1cK	01 04 14.97 ± 0.06	02 10 55.8 ± 0.8	4.8 ± 1.7	4.8 ± 1.7	–

Table 5. Continuum sources detected in WLM: label, coordinates, peak and integrated flux density, and spectral index between 1.4 and 22 GHz (with $S \propto \nu^{\alpha}$) derived for those sources detected with the SRT at *K* band having a counterpart source in the NVSS (see Section 4.1).

Label	RA (J2000)	Dec. (J2000)	Peak (mJy beam^{-1})	Integrated (mJy)	$\alpha_{1.4}^{22}$
WC1C	00 01 35.8 ± 0.8	− 15 21 37 ± 11	4.0 ± 0.4	4.0 ± 0.6	
WC2C	00 02 08.9 ± 1.8	− 15 37 46 ± 27	1.7 ± 0.4	1.7 ± 0.6	
WC3K	00 01 36.0 ± 0.8	− 15 26 22 ± 11	6 ± 2	6 ± 2	–
WC4K	00 01 46.8 ± 0.6	− 15 30 08 ± 9	8 ± 2	8 ± 2	–
WC5aK	00 01 53.0 ± 0.5	− 15 31 31 ± 8	9 ± 2	9 ± 2	–
WC5bK	00 01 46.6 ± 0.5	− 15 31 46 ± 7	10 ± 2	10 ± 2	–
WC6K	00 01 55.8 ± 0.8	− 15 34 51 ± 12	6 ± 2	6 ± 2	–
WC7K	00 02 03.3 ± 0.8	− 15 22 28 ± 11	6 ± 2	6 ± 2	–
WC8K	00 02 19.8 ± 0.4	− 15 33 43 ± 5	13 ± 2	13 ± 2	–

C and *K* bands is ∼5 per cent (e.g. Battistelli et al. 2019) and ∼15 per cent (this work),[6] respectively. For unresolved sources, all parameters were determined fitting a two-dimensional Gaussian with AIPS task JMFIT. In the Gaussian fitting process neither the major nor minor axis sizes were allowed to be smaller than the beam size. For resolved sources, the peak position and flux density were obtained, as before, using JMFIT, while the integrated flux density was estimated using the task TVSTAT over a polygon enclosing the emission down to the 3σ level. The errors on the peak positions were directly provided by the task JMFIT. The uncertainty on the peak flux densities has been conservatively assumed to be the noise of the maps, while that of the integrated ones was computed using the formula reported in Panessa et al. (2015, their section 3). In both cases, when the value obtained was less than the uncertainty on the absolute flux density calibration, the uncertainty was assumed to be 5 per cent and 15 per cent, for *C* and *K* bands, respectively.

[6]This uncertainty at *K* band has been estimated by applying the same flux calibration performed on the target using 3C 286 to a handful of primary calibrators observed during the observations of NGC 6822 (in particular, 3C 48, 3C 147, and 3C 295). The measured flux densities have been compared with those obtained using the standard equations and coefficients reported in Perley & Butler (2013). Our estimate is consistent with the value (10 per cent) reported by Loru et al. (2019). Our larger uncertainty is likely related to worse average weather conditions and/or the low-elevation of the source(s) during the observations.

In addition, our observation allowed us to obtain Full Stokes information at *C* band ($\nu \sim 6.7$ GHz), and hence, to obtain the percentage of polarization of the radio emission at *C* band. The left-hand panels of Figs 1–3 show electric field polarization vectors overlaid on the *C*-band total intensity images. The length of the vectors is proportional to the polarization percentage, while their orientation represents the polarization angle. The fractional polarization shown is above $3\sigma_{\rm FPOL}$. The uncertainty on the fractional polarization ranges from 1 to 20 per cent, depending on the target and on the position within the map. The error on the polarization angle is less than 10°.

As mentioned in Section 2, the *C*- and *K*-band cubes for our three galaxies were searched for methanol and water maser emission lines, respectively. At *C* band, no feature has been found above a 4σ level ($1\sigma \approx 60$ mJy chan^{-1} for a 4-km s^{-1} wide channel; see also Table 7). No water maser detection has been found above a 7σ level ($1\sigma \approx 100$ mJy chan^{-1} for a 1.2-km s^{-1} wide channel; see also Table 7).

4 DISCUSSION

4.1 Radio continuum sources

The RC maps produced by averaging in frequency the radio data cubes show the presence of several RC sources both at *C* and *K* bands. As discussed in two past works by Chyży et al. (2003, 2011), and, more recently, by Hindson et al. (2018), some of these sources may be unrelated to the target objects, being emission produced by background sources. In order to try evaluating which sources belong to the target galaxies, we have derived their spectral index, considered polarization properties and compared our RC maps with those taken at other frequencies, e.g. radio, optical, and UV.

In order to derive the spectral indices of the sources, we have compared our SRT *K*-band maps with those taken from the NRAO VLA Sky Survey (NVSS) at 1.4 GHz (Condon et al. 1998). The resolution of the two maps is comparable, 50 and 45 arcmin for the SRT and VLA images, respectively, allowing to identify the main centres of RC emission at both frequencies. The last columns of Tables 3–5 report the spectral index between 1.4 and 22 GHz, $\alpha_{1.4}^{22}$ (with $S \propto \nu^{\alpha}$) of the sources detected above a 3σ level, at both frequencies. The error on the spectral indices has been computed, using the standard error propagation formula, from the errors reported for the sources at *K* band (Tables 3–5) and those obtained from the NVSS source catalogue (Condon et al. 1998).

A preliminary association of the RC sources with the galaxies is mainly based on the presence (or absence) of optical/UV/FUV counterparts (Figs 4, 5, and 6). In NGC6822, the target labelled NC3C is clearly offset w.r.t. the optical body of the galaxy. This and the presence of linear polarization (up to $\sim 20 \pm 5$ per cent) hints at a non-thermal nature of the emission. This makes the object a background source candidate. Similarly, background source candidates are also sources IC1C in IC1613, and WC1C, WC2C, and WC8K in WLM. The other RC sources detected in the three targets lie to some extent within the optical body of the galaxies. However, for NGC6822, NC4C shows linear polarization in the northeastern extension with a percentage between 10 ± 5 and 22 ± 10, and also, although at a lower level (5 ± 1 per cent), close to the source peak. Indeed, NC4C is also resolved into, at least, two sources at *L*- and *K*-bands, both with negative spectral index (see Table 3), thus hinting at a non-thermal nature of the emission. This, together with the lack of evident counterparts at other wavelengths, conceivably makes NC4C a background object. The same conclusion was also reached by Chyży et al. (2003). Notably, at resolution and frequencies comparable to those in our study, polarization fractions of the order of some 10 per cent (as also found in NC3C, see above) are not unusual in radio sources, and, for example, in the case of tailed radio galaxies, are expected to increase along the tail reaching values above 50 per cent (see e.g. Feretti et al. 1998). All other sources in NGC6822 are either

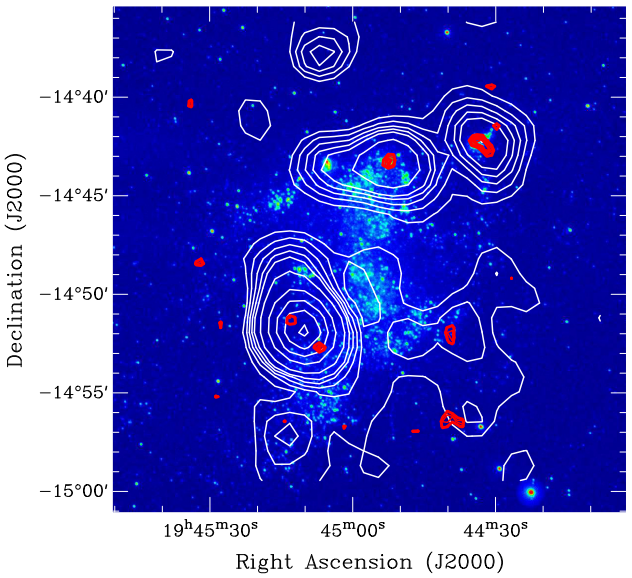

Figure 4. Combination of an FUV Galex map of NGC 6822 with the SRT RC *C* (white) and *K* (red) band contour maps overlaid. Contour levels are 0.65 × (2, 4, 6, 8, 10, 15, 25, 35, 45, 55) mJy and 2 × (3, 3.5, 4, 4.5, 5) mJy, for the *C* and *K* bands, respectively.

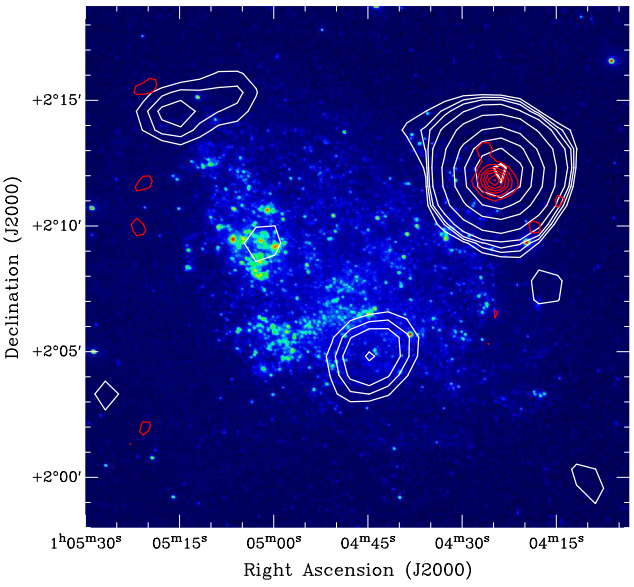

Figure 5. Combination of an FUV Galex map of IC 1613 with the SRT RC *C* (white) and *K* (red) band contour maps overlaid. Contour levels are 1.0 × (2, 3, 4, 6, 12, 24, 36, 48, 60) mJy and 1.7 × (3, 6, 9, 12, 15, 18, 21) mJy, for the *C* and *K* bands, respectively.

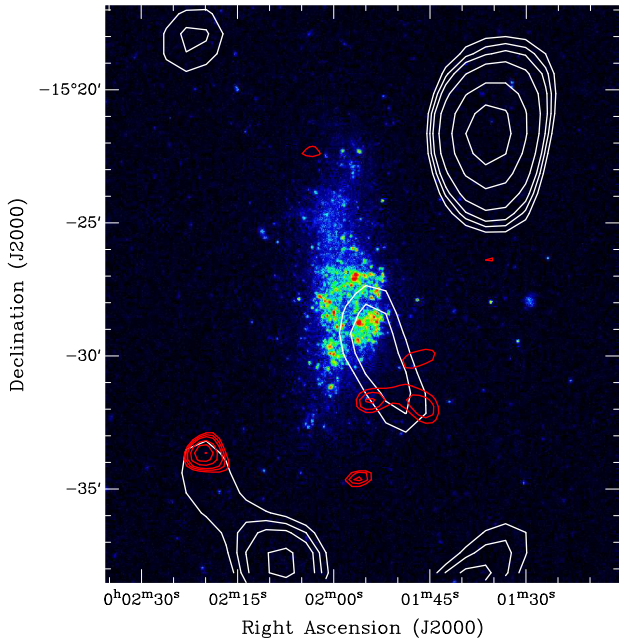

Figure 6. Combination of an FUV Galex map of WLM with the SRT RC *C* (white) and *K* (red) band contour maps overlaid. Contour levels are 0.4 × (2, 2.5, 3, 4, 6, 8) mJy and 1.9 × (3, 3.5, 4, 5, 6, 7) mJy, for the *C* and *K* bands, respectively.

related to the target objects or are of ambiguous nature.[7] In the case of IC1613, the detected RC sources are all of ambiguous nature. Indeed, the case of IC1C is quite peculiar. The source is linearly polarized (between 5 and 10 per cent) and is resolved into three centres of emission at *K* band. However, the spectral index of the brightest component is flat, possibly indicating a thermal origin. Thus, despite the source being at the outskirts of the optical body of the galaxy, it cannot be confidently classified as a background source, although in the following discussion it will be treated as such. For WLM, the spatial distance of the RC sources to the main optical emitting regions favours a scenario in which these sources are unrelated to the galaxy, with the exception of sources WC4K, and WC5K (a and b), that have some (weak) optical counterparts.

In Table 6, we report the *C*-band RC flux of the target galaxies derived by integrating over an area covering the optical body of the galaxy. Integrated fluxes were measured both including the emission coming from all sources in the map and subtracting the contribution by the most likely background source candidates (see the discussion above).[8] Uncertainties on the integrated fluxes were computed using the formula reported in Panessa et al. (2015, their section 3). In all cases, the values obtained were larger than the uncertainty on the absolute flux density calibration, i.e. 5 per cent (see Section 3). The star formation rate (SFR) of each galaxy from the emission at 6.7 GHz, computed by using the following RC–SFR relation, taken from Hindson et al. (2018, their equation 10), is also reported:

$$\frac{L_{\rm RC}}{\rm W\,Hz^{-1}} = 10^{A}\left(\frac{\rm SFR}{\rm M_{\odot}\,yr^{-1}}\right)^{n}, \quad (1)$$

where A and n are the best-fitting parameters for the RC–SFR relation, derived by Hindson et al. for their data using different approaches (their section 4.6). For our estimates, we used an average value of these parameters [Hindson et al. (2018, their table 6)], of 20.1 and 0.9, for A and n, respectively.

In Table 6, we also report the computed values of the SFR in the three galaxies, obtained from the 1.4-GHz luminosity through the equation by Hopkins, Schulte-Ladbeck & Drozdovsky (2002, and references therein; their equation 2):

$$\rm SFR = 5.5 \times \left(\frac{\mathit{L}_{1.4\,GHz}}{4.6 \times 10^{21}\,W\,Hz^{-1}}\right) M_{\odot}\,yr^{-1}. \quad (2)$$

The 1.4 GHz luminosities are derived from the 6.7 GHz luminosities, assuming a spectral index of 0.75 (Gioia, Gregorini & Klein 1982).[9]

The last column of Table 6 reports the SFR of the three targets reported by Mateo (1998) and derived by using the H α emission.

Reported errors for the luminosities and SFRs take into account, through the standard errors propagation equation, both the flux density uncertainties and those for the galaxy distance (see Table 1). When comparing the SFRs obtained in this work with those reported, without an associated uncertainty, by Mateo (1998), it has, however, to be considered that the distances used for the galaxies are the same.

The SFRs derived at radio frequencies from equations (1) and (2) agree fairly well. For NGC 6822 all RC-based SFRs are (significantly) lower than that obtained with H α. For IC 1613, instead, excluding the RC emission background source candidates in the SFR computation provides a better match with the H α-based SFR, possibly confirming that IC1C is indeed not associated with the galaxy. For WLM, SFRs derived from the RC are consistent with those derived by using the H α emission only when considering all the emission present in the field as belonging to the galaxy (that, as said before, is unlikely). Overall, however, for two out of our three targets, the global SFRs derived by 'optical means' are higher than those derived by us using RC data. This is consistent with the conclusions of Hindson et al. (2018). Indeed, they find that their targets (i.e. dwarf galaxies) follow the theoretical predictions of the RC–SFR relation only in individual regions of enhanced RC emission but, apparently, not when considering the entire optical discs of the galaxies.

4.2 The paucity of methanol and water masers in dwarf galaxies

For this project, for the first time, the full optical body of the galaxies NGC 6822, IC 1613, and WLM was searched for spectral line emission at 6.7 and 22 GHz. In the past, only water maser emission was searched for in these galaxies but these searches were limited to individual regions, typically associated with enhanced H α or FIR emission (see Brunthaler et al. 2006, hereafter BHB,

[7]We define as ambiguous those sources for which it is not possible, from the information available to date, to confidently determine or exclude their association to the galaxies

[8]For NGC 6822, we subtracted the contribution of sources NC3C and NC4C. For IC 1613, we removed the flux pertaining to IC1C. For WLM, both RC sources, WC1C and WC2C were excluded.

[9]This value is the average spectral index value estimated for spiral galaxies. For dwarf irregular galaxies, flatter RC spectra than those of 'normal' spiral galaxies, have indeed also been suggested (e.g. Klein & Gräve 1986). This would, however, reduce the extrapolated 1.4-GHz luminosities, and the corresponding SFRs, thus further reinforcing our considerations.

Table 6. Galaxy name, integrated 6.7 GHz flux and luminosity (upper line: including all sources; lower line: excluding background sources) and corresponding 1.4 GHz flux and luminosity (derived assuming a spectral index of 0.75; $S \propto \nu^{\alpha}$), SFRs estimated using equation (1), equation (2), and from extinction-corrected Hα fluxes (from Mateo 1998). For details, see also Section 4.1.

Source	$S_{\rm RC}^{6.7\,\rm GHz}$ (mJy beam^{-1})	$L_{\rm RC}^{6.7\,\rm GHz}$ (Watt Hz^{-1})	$S_{\rm RC}^{1.4\,\rm GHz}$ (mJy beam^{-1})	$L_{\rm RC}^{1.4\,\rm GHz}$ (Watt Hz^{-1})	$\rm SFR_{RC1}^{a}$ ($\rm M_{\odot}yr^{-1}$)	$\rm SFR_{RC1}^{b}$ ($\rm M_{\odot}yr^{-1}$)	$\rm SFR_{H\alpha}^{c}$
NGC 6822	96 ± 5	$(2.8 \pm 0.5) \times 10^{18}$	312 ± 16	$(9 \pm 2) \times 10^{18}$	0.014 ± 0.003	0.011 ± 0.002	0.06
	44 ± 5	$(1.4 \pm 0.3) \times 10^{18}$	141 ± 16	$(4.0 \pm 0.8) \times 10^{18}$	0.006 ± 0.001	0.005 ± 0.001	
IC 1613	81 ± 4	$(4.8 \pm 0.5) \times 10^{18}$	263 ± 13	$(1.5 \pm 0.2) \times 10^{19}$	0.026 ± 0.003	0.018 ± 0.002	0.003
	16 ± 5	$(1.0 \pm 0.3) \times 10^{18}$	53 ± 16	$(3 \pm 1) \times 10^{18}$	0.004 ± 0.002	0.004 ± 0.001	
WLM	9 ± 1	$(9 \pm 1) \times 10^{17}$	28 ± 1	$(2.9 \pm 0.3) \times 10^{18}$	0.0041 ± 0.0007	0.0034 ± 0.0004	0.003
	3 ± 1	$(1 \pm 1) \times 10^{17}$	10 ± 2	$(10 \pm 3) \times 10^{17}$	0.0012 ± 0.0006	0.0012 ± 0.0003	

[a]From equation (1).
[b]From equation (2).
[c]From Mateo (1998).

and references therein). As mentioned in Section 1, the possible absence of an optical counterpart associated with a maser source, makes the need to create fully sampled spectroscopic images of the entire optical extension of the galaxies particularly important, in order to confidently assess the occurrence of maser emission in the target galaxy. For the three targets of our study, the lack of confident line detections, both at *C* and *K* bands, indicates a general absence of (strong) maser emission in dwarf galaxies. In the following two subsections, we try to associate the aforementioned absence to the main peculiarities of dwarf galaxies.

4.2.1 The modest star-forming rate

For water masers, our result confirms the conclusions obtained by BHB. Indeed, for water masers, their study indicates that a value for the expected number (N) of masers can be computed using the luminosity function (LF) for H_2O masers in our Galaxy, empirically derived by Greenhill et al. (1990) and accounting for the different SFRs of the target galaxy and that of the MW.[10] For H_2O masers, the expected number of sources with an isotropic luminosity larger than a certain value, $L_{\rm H_2O}$, is:

$$N_{\rm expected}^{\rm H_2O} = 10^{\{-0.6\times[1+\log(L_{\rm H_2O})]\}} \times (\rm SFR_{target}/SFR_{Milky\ Way}), \quad (3)$$

where the luminosity in the 22 GHz line $L_{\rm H_2O}$ (in $\rm L_{\odot}$) is taken as the (4σ) detection threshold of our observations, S (in Jy), derived from the maser line width assumed to be equal to the velocity width of the channel (Δv; 1.2 km s^{-1}, in our case), and from the distance (in Mpc) of our target galaxy, using the equation

$$L_{\rm H_2O} = 0.023 \times S \times \Delta v \times D^2. \quad (4)$$

For example, with a 3σ detection threshold of 30 mJy chan^{-1} (millyJansky/channel) for a 1-km s^{-1} wide channel, and using SFRs for the MW and M 31 of 4 $\rm M_{\odot}yr^{-1}$ (Diehl et al. 2006; from the frequency of core-collapse supernovae derived by gamma-ray measurements) and 0.35 $\rm M_{\odot}yr^{-1}$ (Walterbos & Braun 1994; from the extinction-corrected Hα luminosity), respectively, we obtain an expected number of maser sources in M 31 of about 3. This number is fully consistent with the water maser detections obtained in M 31 by Darling (2011) and Darling et al. (2016). Similarly consistent results are also found for the other LG galaxies where water masers have been found,[11] with the exception of IC 10 in which an overabundance of masers with respect to the expected number is detected (see BHB, and references therein). Table 7 reports the number of water masers expected for the three galaxies in our study, with a luminosity larger than the threshold corresponding to the 4σ level of our cubes. As evident, the expected number is small for all galaxies (close to zero for IC 1613 and WLM). Indeed, for NGC 6822, lowering the luminosity threshold by an order of magnitude (2–3 orders of magnitude are instead required for dwarfs with SFRs similar to those of IC 1613 and WLM) would bring the expected number to unity, opening the possibility for a detection but this would require an extremely long observation, when not led with the aid of a multifeed receiver or with an extremely sensitive facility.

For methanol masers, a relation similar to equation (3) can also be derived by using the information reported in Quiroga-Nuñez et al. (2017). Using their value for the slope of the LF ($\alpha = -1.43$) and the reported total number of Galactic methanol masers of 1300 (Quiroga-Nuñez et al. 2017), computed integrating between 10^{-8} and 10^{-3} $\rm L_{\odot}$ (from Pestalozzi et al. 2007), the complete relation for the LF can be now be expressed as $f(L) = 0.2 \times L^{-1.43}$. Hence, the expected number of 6.7-GHz methanol masers with an isotropic luminosity larger than a certain value, $L_{\rm CH_3OH}$, is:

$$N_{\rm expected}^{\rm CH_3OH} = 10^{\{-0.4\times[0.8+\log(L_{\rm CH_3OH})]\}} \times (\rm SFR_{target}/SFR_{Milky\ Way}), \quad (5)$$

where $L_{\rm CH_3OH}$ (in $\rm L_{\odot}$) is taken as the (4σ) detection threshold of our observation, S (in Jy), from the maser line width assumed equal to the velocity width of the channel (Δv; 4.1 km s^{-1}, in our case), and from the distance (in Mpc) to our target galaxy, using the equation

$$L_{\rm CH_3OH} = 0.0069 \times S \times \Delta v \times D^2. \quad (6)$$

Table 7 reports the number of methanol masers expected for the three galaxies of our study, with a luminosity larger than the threshold corresponding to the 4σ level of our cubes. Also in this case, the expected numbers are small, well below unity.

For the computation of the expected number of both water and methanol masers, we used the SFRs derived from extinction-corrected Hα fluxes, as reported in Mateo (1998, also see Table 6). Using the SFRs derived by us from the RC (Table 6) would yield

[10]The ratio is based on the assumption that the rates of maser production and star formation are roughly proportional. This assumption is plausible when, as in this case, we are considering exclusively masers associated with star formation. Indeed, there is no AGN related H_2O (mega)maser in the LG.

[11]Slightly different numbers and conclusions are, however, reached for the Large and Small Magellanic Clouds by Breen et al. (2013).

Table 7. Galaxy name (col. 1); average 1σ rms noise levels in the *C*-band and *K*-band cubes (cols. 2 and 6); methanol and water maser luminosity detection limits (cols. 3 and 7), computed from equations (6) and (4), respectively, using the 4σ rms levels in the cubes and a channel width of 4 and 1.2 km s^{-1}, respectively; number of expected methanol and water masers (cols. 4 and 8), derived from equations (5) and (3), respectively; number of methanol and water masers detected (cols. 5 and 9).

Source	rms_{CH_3OH} (mJy)	L_{CH_3OH} ($L_\odot$)	$N^{exp,\,a}_{CH_3OH}$	$N^{det}_{CH_3OH}$	rms_{H_2O} (mJy)	L_{H_2O} ($L_\odot$)	$N^{exp,\,a}_{H_2O}$	$N^{det}_{H_2O}$
NGC 6822	60	1.6×10^{-3}	0.1	0	80	2.2×10^{-3}	0.1	0
IC 1613	60	3.3×10^{-3}	0.004	0	70	3.9×10^{-3}	0.005	0
WLM	65	6.3×10^{-3}	0.003	0	160	15.5×10^{-3}	0.002	0

[a]The expected maser numbers are computed using the SFRs derived from extinction-corrected Hα fluxes, as reported in Mateo (1998, see also Table 6).

even lower values for the expected numbers and would not change our conclusions.

4.2.2 *The low metallicity*

Dwarf irregular galaxies are relatively low mass, gas-rich, metal-poor, and are sometimes forming stars as shown by their H II regions (e.g. Lee, Skillman & Venn 2005). Indeed, our three targets have low metallicities, with 12 + log(O/H) values of 8.0, 7.9, and 7.8, for NGC 6822 (Schruba et al. 2017), IC 1613 (Bresolin et al. 2007), and WLM (Rubio et al. 2015), respectively. This corresponds approximately to 15–20 per cent of the solar value (∼8.7, from Asplund et al. 2009). While, as discussed in the previous section, the SFRs for these galaxies are already lower than those of regular spirals, resulting in low expected numbers of masers in dwarf galaxies, it is reasonable to assume that the low oxygen and carbon abundances, together with a low abundance of other processed elements and dust, may influence the possibility to have a large fraction of water and methanol molecules, further reducing the possibility to have maser emission from these species. The chemical modelling of dark clouds in the Magellanic clouds by Millar & Herbst (1990) indicates, however, that the scaling between molecular and elemental abundances, except for the CO molecule, does not follow a simple pattern and that the molecular abundances depend on the varying C, O, and N elemental abundances in the models in a complex manner. From the observational point of view, the CO content and distribution in low-metallicity dwarf galaxies have been recently studied using ALMA observations by Rubio et al. (2015) and Schruba et al. (2017). Their conclusions mainly point to the presence of compact CO clumps, with small radii, narrow-line width, and low filling factor across these galaxies. The confined nature of the CO emission agrees with a scenario invoking a lack of dust shielding that would push CO emission deep into molecular clouds in low-metallicity objects. Within this framework, the same absence of dust shielding, and, correspondingly, smaller fraction of dust grains could prevent the formation of some molecules, as methanol and water are typically formed via reactions on grains surfaces. It could also increase the efficiency of photodissociation and photoionization on the molecules after their formation caused by external radiation. This seems to be true for the methanol molecule, thought to be produced by the hydrogenation of CO on dust grains and released into the gas phase by thermal and/or non-thermal desorption (e.g. Watanabe & Kouchi 2002). Indeed, a low abundance of dust grains would then make the methanol formation inefficient, explaining the lack of detected methanol lines in the LMC and IC 10 (Nishimura et al. 2016, and references therein). Hence, it is not far-fetched to assume that a similar scenario applies also to the water molecule, although this hypothesis has not, to our knowledge, been investigated yet. If this scenario is confirmed, the expected number of maser sources suggested by equations (3) and (5) would provide upper limits.

5 CONCLUSIONS

During Spring 2016, we obtained OTF (single-feed) maps of the continuum and spectral line radio emission over the full optical extents of 14 LG dwarf galaxies, belonging to two highly symmetric dynamical planar structures, with the SRT, at *C* and *K* bands. The data for the first three galaxies, NGC 6822, IC 1613, and WLM, were reduced and analysed in order to obtain the distribution and intensity of the RC emission from the targets and, to search, for the first time across the entire extension of the galaxies, for methanol and water (maser) sources to be used for follow-up VLBI proper motion studies. We summarize our results and conclusions as follows:

(i) RC emission has been detected in all maps, mainly coming from discrete sources, although a diffuse component is also seen in the *C*-band map of NGC 6822. Spectral indices for the sources have been estimated with values consistent with a mix of thermal and non-thermal origin. Polarization properties at *C* band have been also inferred, showing that some sources are linearly polarized with percentages higher than 20 per cent. Indeed, some of the RC sources have been found unrelated to the galaxies and are likely produced by background objects.

(ii) Global SFRs have been derived from the RC emission detected from the galaxies. They have been found to be, on average, lower than those obtained at other wavelengths. This may suggest that, as also concluded by other authors, dwarf galaxies do not follow the theoretical predictions of the RC–SFR relation when the whole optical discs are considered, while the correlation holds for individual regions of enhanced RC emission.

(iii) No 6.7-GHz methanol and 22-GHz water maser emission has been detected in the three targets, with isotropic luminosity above a few thousandths of solar luminosities. This is consistent with past studies that indicate that the number of maser sources (associated with star formation activity) in a galaxy should decrease with its SFR. In addition, a low metallicity may reduce the abundance of the masing molecular species, because of a smaller fraction of dust grains where such molecules typically form and from which molecules are shielded by the strong radiation field. Hence, the combination of low SFR and low abundance of heavy elements in irregular dwarf galaxies could work against a widespread presence of maser sources in this class of galaxies.

Overall, our study has further shown the potential of the SRT in performing OTF fully sampled spectropolarimetric maps of extended sources in the sky. It has, however, also pointed out the necessity to perform sufficiently sensitive measurements (between 1 and 3 orders of magnitude deeper, depending on the target's

SFR, than the one reported in this work) when weaker or elusive star formation related (maser) lines are searched for in dwarf galaxies. This necessarily implies extremely long integration times, especially at high frequencies, something unsustainable for modern, often oversubscribed facilities. Therefore, the use of multifeed receivers in this kind of studies becomes mandatory. Indeed, a 7-feed *K*-band receiver has been recently offered also for spectropolarimetric measurements at the SRT, making deep spectral line surveys in extended objects now possible. In addition, the SKA telescope and the ng-VLA, with their unique sensitivity, will ultimately be game-changers in this kind of studies.

ACKNOWLEDGEMENTS

The SRT ESP activities were made possible thanks to the invaluable support of the entire SRT Operations Team. In particular, we would like to thank Ettore Carretti for all the work done as Officer-in Charge of the SRT during the ESP, and Franco Buffa for promptly providing us with the relevant weather information during observations. We thank the anonymous referee for his/her comments. We are grateful to Federica Govoni for useful discussion, and to Luis Quiroga-Nuñez for sharing information on the Galactic methanol maser luminosity function. The Sardinia Radio Telescope is funded by the Department of University and Research (MIUR), Italian Space Agency (ASI), and the Autonomous Region of Sardinia (RAS) and is operated as National Facility by the National Institute for Astrophysics (INAF). The development of the SARDARA backend has been funded by the Autonomous Region of Sardinia (RAS) using resources from the Regional Law 7/2007 'Promotion of the scientific research and technological innovation in Sardinia' in the context of the research project CRP-49231 (year 2011, PI Possenti): 'High resolution sampling of the Universe in the radio band: an unprecedented instrument to understand the fundamental laws of the nature'. This publication is partly based on observations with the 100-m telescope of the MPIfR (Max-Planck-Institut für Radioastronomie) at Effelsberg. This research has made use of the NASA/IPAC Extragalactic Database (NED), which is operated by the Jet Propulsion Laboratory, California Institute of Technology, under contract with the National Aeronautics and Space Administration.

REFERENCES

Amiri N., Darling J., 2016, ApJ, 826, 136
Argon A. L., Greenhill L. J., Moran J. M., Reid M. J., Menten K. M., Henkel C., Inoue M., 1994, ApJ, 422, 586
Asplund M., Grevesse N., Sauval A. J., Scott P., 2009, ARA&A, 47, 481
Baan W. A., Haschick A., 1994, ApJ, 424, L33
Battistelli E. S. et al., 2019, ApJ, 877, L31
Becker R., Henkel C., Wilson T. L., Wouterloot J. G. A., 1993, A&A, 268, 483
Bolli P. et al., 2015, J. Astron. Instrum., 4, 450008
Breen S. L., Lovell J. E. J., Ellingsen S. P., Horiuchi S., Beasley A. J., Marvel K., 2013, MNRAS, 432, 1382
Bresolin F., Urbaneja M. A., Gieren W., Pietrzyński G., Kudritzki R., 2007, ApJ, 671, 2028
Brunthaler A., Reid M. J., Falcke H., Greenhill L. J., Henkel C., 2005, Science, 307, 1440
Brunthaler A., Henkel C., de Blok W. J. G., Reid M. J., Greenhill L. J., Falcke H., 2006, A&A, 457, 109 (BHB)
Brunthaler A., Reid M. J., Falcke H., Henkel C., Menten K. M., 2007, A&A, 462, 101
Buck T., Dutton A. A., Macciò Andrea V., 2016, MNRAS, 460, 4348
Chyży K. T., Knapik J., Bomans D. J., Klein U., Beck R., Soida M., Urbanik M., 2003, A&A, 405, 513
Chyży K. T., Weżgowiec M., Beck R., Bomans D. J., 2011, A&A, 529, A94
Condon J. J., Cotton W. D., Greisen E. W., Yin Q. F., Perley R. A., Taylor G. B., Broderick J. J., 1998, AJ, 115, 1693
Darling J., 2011, ApJ, 732L, 2
Darling J., Gerard B., Amiri N., Lawrence K., 2016, ApJ, 826, 24
Diehl R. et al., 2006, Nature, 439, 45
Felli M. et al., 2007, A&A, 476, 373
Feretti L., Giovannini G., Klein U., Mack K. -H., Sijbring L. G., Zech G., 1998, A&A, 331, 475
Fritz T. K., Battaglia G., Pawlowski M. S., 2018, A&A, 619, 103
Gaia Collaboration, 2018, A&A, 616, A12
Gillet N., Ocvirk P., Aubert D., Knebe A., Libeskind N., Yepes G., Gottlöber S., Hoffman Y., 2015, ApJ, 800, 34
Gioia I. M., Gregorini L., Klein U., 1982, A&A, 116, 164
Govoni F. et al., 2017, A&A, 603, A122
Greenhill L. J., Moran J. M., Reid M. J., Gwinn C. R., Menten K. M., Eckart A., Hirabayashi H., 1990, ApJ, 364, 513
Greenhill L. J., Moran J. M., Reid M. J., Menten K. M., Hirabayashi H., 1993, ApJ, 406, 482
Henkel C., Greene J.-E., Kamali F., 2018, Proc. IAU Symp. 336, Extragalactic Maser Surveys. Kluwer, Dordrecht, p. 69
Hindson L. et al., 2018, ApJS, 234, 29
Hopkins A. M., Schulte-Ladbeck R. E., Drozdovsky I. O., 2002, AJ, 124, 862
Ibata R. A. et al., 2013, Nature, 493, 62
Karachentsev I. D., Makarov D. I., Kaisina E. I., 2013, ApJ, 145, 101
Klein U., Gräve R., 1986, A&A, 161, 155
Lee H., Skillman E. D., Venn K. A., 2005, ApJ, 620, 223
Loru S. et al., 2019, MNRAS, 482, 3857
Mateo M., 1998, ARA&A, 36, 435
McConnachie A. W., 2012, AJ, 144, 4
Melis A. et al., 2018, J. Astron. Instrum., 7, 1850004
Metz M., Kroupa P., Libeskind N. I., 2008, ApJ, 680, 287
Millar T. J., Herbst E., 1990, MNRAS, 242, 92
Müller O., Pawlowski M. S., Jerjen H., Lelli F., 2018, Science, 359, 534
Murgia M. et al., 2016, MNRAS, 461, 3516
Nishimura Y., Shimonishi T., Watanabe Y., Sakai N., Aikawa Y., Kawamura A., Yamamoto S., 2016, ApJ, 829, 94
Panessa F. et al., 2015, MNRAS, 447, 1289
Pawlowski M. S., Kroupa P., 2013, MNRAS, 435, 2116
Pawlowski M. S., Kroupa P., Jerjen H., 2013, MNRAS, 435, 1928
Pawlowski M. S., McGaugh S. S., Jerjen H., 2015, MNRAS, 453, 1047
Pawlowski M. S., Pflamm-Altenburg J., Kroupa P., 2012, MNRAS, 423, 1109
Perley R. A., Butler B. J., 2013, ApJS, 204, 19
Pestalozzi M. R., Chrysostomou A., Collett J. L., Minier V., Conway J., Booth R. S., 2007, A&A, 463, 1009
Prandoni I. et al., 2017, A&A, 608, 40
Quiroga-Nuñez L. H., van Langevelde H. J., Reid M. J., Green J. A., 2017, A&A, 604, A72
Rubio M., Elmegreen B. G., Hunter D. A., Brinks E., Cortés J. R., Cigan P., 2015, Nature, 525, 218
Schruba A. et al., 2017, ApJ, 835, 278
Silich S., Lozinskaya T., Moiseev A., Podorvanuk N., Rosado M., Borissova J., Valdez-Gutierrez M., 2006, A&A, 448, 123
Sjouwerman L. O., Murray C. E., Pihlström Y. M., Fish V. L., Araya E. D., 2010, ApJ, 724, L158
Surcis G., Vlemmings W. H. T., Curiel S., Hutawarakorn Kramer B., Torrelles J. M., Sarma A. P., 2011, A&A, 527, 48
Walterbos R. A. M., Braun R., 1994, ApJ, 431, 156
Watanabe N., Kouchi A., 2002, ApJ, 571, L173

Table A1. Tentative water maser features in NGC 6822, IC 1613, and WLM. The heliocentric velocity of the galaxies from McConnachie (2012), V_{Sys}, are −57, −233, and −130 km s^{-1}, for NGC 6822, IC 1613, and WLM, respectively. The uncertainty on the feature coordinates and velocities are given by the map cell size (15 arcsec) and channel width (1.2 km s^{-1}), respectively. The uncertainty on the feature peak flux density is conservatively assumed to be the spectrum noise at the feature position (column 7).

Feature code	RA (J2000)	Dec. (J2000)	$V_{Feat.}$ (km s^{-1})	$\lvert V_{Feat.}-V_{Sys}\rvert$ (km s^{-1})	Peak flux density (mJy)	Spectral noise (mJy)	SNR
			NGC 6822				
NL1K	19 44 31.9	−14 41 42	−5	52	543	127.4	4.3
NL2K	19 44 37.0	−14 55 12	15	72	384	85.8	4.5
NL3K	19 44 40.1	−14 48 12	−32	25	349	84.6	4.1
NL4K	19 44 46.3	−14 46 12	−183	126	398	86.3	4.6
NL5K	19 45 07.0	−14 52 42	62	119	440	107.4	4.1
			IC 1613				
IL1K	01:04:21.8	02:09:19	−99	134	276	66.4	4.2
IL2K	01:04:22.8	02:13:49	−75	158	281	69.6	4.0
IL3K	01:04:52.8	02:04:04	−115	118	286	70.6	4.0
IL4K	01:05:10.8	02:12:04	−352	119	384	65.0	5.9
			WLM				
WL1K	00 01 49.8	−15 26 54	−152	22	663	162.0	4.1
WL2K	00 02 05.4	−15 27 39	−139	9	660	159.7	4.1
WL3K	00 02 06.4	−15 25 39	−299	169	691	162.1	4.3

APPENDIX A: WATER MASER TENTATIVE DETECTIONS

In our search for maser sources, we considered as tentative detections those features that were detected at an SNR level between 4σ and 7σ (see Section 2). While no candidate detections were found at *C* band, a small number (12) of tentative water maser detections have been found, at *K* band, in each of the three galaxies, among which, one in IC 1613, is seen at a 5.9σ level (Table A1). The extremely low number of maser sources expected to be detectable in the galaxies (Section 4) makes, however, highly unlikely that all these detections are real.

From a statistical point of view, we can estimate the probability that the 5.9σ tentative line detection, labelled IL4K, in IC 1613, obtained by us in a single channel is spurious or not. Assuming a Gaussian distribution, the number of possibilities to have an $n\sigma$ spurious event in a galaxy is given by the number of positions/pixels (58 × 58 or 28 × 28, for NGC 6822/IC 1613 and WLM, respectively) times the number of channels (326) searched for a feature, times the probability to have an $n\sigma$ spurious event. For a 5.9σ significance, the expected number of spurious detections are 0.004, 0.004, and 0.001, for NGC 6822, IC 1613, and WLM, respectively. For a 4–5σ significance, instead, the expected number of spurious detections ranges between 72 (4σ) and 0.65 (5σ), for NGC 6822 or IC 1613, and between 16 (4σ) and 0.15 (5σ) for WLM. Therefore, while some of the tentative detections at 4–5σ may indeed be expected to be factitious, the 5.9σ tentative detection can be considered as a significant maser candidate.

From an observational/astrophysical point of view, the IL4K water maser source line IC 1613 is detected in a single channel of 92 kHz (∼1.2 km s^{-1} at 22 GHz) with a peak flux density of 0.38 Jy, thus corresponding to an isotropic luminosity of about 0.005 L$_\odot$. The velocity of the feature is blueshifted w.r.t. the systemic velocity of the galaxy by ∼120 km s^{-1} (Table A1) and the location of the maser line does not coincide (although it is very close to) any obvious centre of activity at FUV or radio wavelengths (see Fig. A1). IL4K, because of its characteristics, may resemble IC 10-NW, one of the two maser sources (somewhat unexpectedly; see Section 4) found in IC 10 (Becker et al. 1993; Argon et al. 1994; Baan & Haschick 1994), another LG dwarf galaxy. A main difference is, however, given by the large offset between the velocity of the maser line in IC 1613 and the systemic velocity of the galaxy, that is not found in the IC10 source. Such a large offset cannot be justified by the gas velocity field of the galaxy derived by interferometric H I measurements that is relatively smooth and with a small velocity dispersion, with the exception of a few intermediate-size bubbles where an expansion velocity of 10–20 km s^{-1} was measured (Silich et al. 2006). The possibility remains that mechanical energy released in the ISM from strong stellar winds, supernova explosions, or bubbles may influence the local velocity field through shocks.

Notably, two other weaker tentative features, labelled NL1K and NL5K, in NGC 6822, have peculiarities that are worth to be mentioned. Indeed, NL1K is located in a particularly active star-forming region to the NW, associated with NC1C (see Fig. 4), and has a velocity offset w.r.t the systemic one of 'only' 52 km s^{-1}. The source NL5K has a much larger velocity offset (∼120 km s^{-1}), but it is coincident with NC4aK, one of the two *K* band sources associated with NC4C, the strongest continuum source in the map (Fig. 4).

Indeed, in order to try confirming the three aforementioned features, we re-observed at the positions of IL4K (on 2019 January 15), and NL1K and NL5K (on 2019 February 14) with the SRT (DDT project #3-19)[12] and with Effelsberg on February 6 (only IL4K). In both cases, the observations were conducted in Position Switching mode with total on-source integration times of about 30 min (for the SRT) and 12 min (for Effelsberg), yielding a similar rms noise of ∼30 mJy beam^{-1} in a 25 and 38 kHz channel, for SRT and Effelsberg, respectively. Oddly, and unfortunately, no line was detected at the velocity of the features originally detected in our ESP project above a 3σ level of 100 mJy chan^{-1}. Strong variability is indeed a possible explanation, given that narrow star formation water maser features are typically highly variable (see e.g. Felli

[12]It should be noted that the SRT was not available for observations from 2016 September to 2018 December because of extraordinary maintenance and subsequent technical/scientific re-comissioning phases.

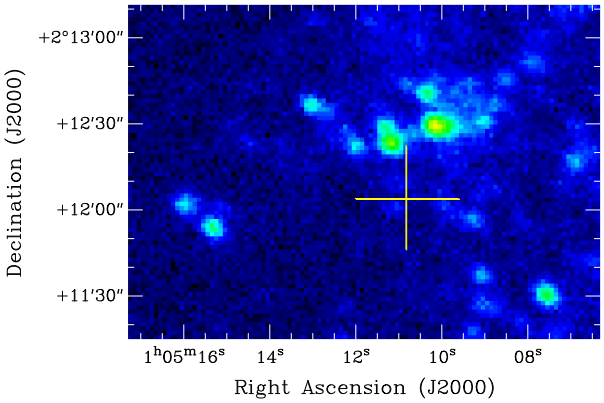

Figure A1. Zoom-in of Fig. 5, showing the FUV Galex map of the region of IC 1613 where the water maser 5.9σ tentative feature has been observed with the SRT. The yellow cross indicates the position of the feature (see Table A1).

et al. 2007). However, the variability scenario would also imply a decrease of more than a factor 3–5 of the flux density in all three features within the same 3 yr period. Hence, the possibility that (some of) the tentative line emission features detected in our survey may be produced by backend artefacts or RFI, rather than having an astrophysical origin, cannot be confidently excluded. Additional follow-up observations of the other 9 tentative detections reported and/or a monitoring of the three aforementioned tentative targets would be therefore advisable.

This paper has been typeset from a TEX/LATEX file prepared by the author.